Ammonia borane-based nanocomposites as solid state hydrogen stores for portable power applications

Laura Bravo Diaz,[a], [b] James M. Hanlon,[a] Marek Bielewski,[b] Aleksandra Milewska,[c] and Duncan H. Gregory.[a]*

Abstract: Ammonia borane (AB) based nanocomposites have been investigated with the aim of developing a promising solid-state hydrogen store that complies with the requirements of a modular polymer electrolyte membrane fuel cell (PEM FC) in a portable power pack system. AB-carbon nanocomposites (prepared *via* ball milling or solution-impregnation) demonstrate improved hydrogen release performance compared to AB itself in terms of onset temperature and hydrogen purity, while maintaining a gravimetric density of more than 5 wt. % H_2. The most promising of these materials is an AB-AC (activated carbon) composite, synthesised *via* solution-impregnation with an optimal dehydrogenation temperature of 96 °C. When combined with an external nickel chloride filter downstream, no evolved gaseous by-products can be detected above 100 ppb. The feasibility of an AB-AC storage tank has been further endorsed by simulations in which the reaction rate and the hydrogen flux was found to be almost constant as the temperature front propagated from the bottom to the top of the tank after initiation.

Introduction

A major challenge facing modern society is to find a sustainable way to overcome our reliance on fossil fuels. Hydrogen is the fuel (energy vector) of choice for high performance fuel cells (FCs), but its potential use for mobile applications is likely only to be realised if advanced solid state storage solutions are developed. A number of solid state materials have been investigated but none yet meets the US Department of Energy (DoE) targets for hydrogen storage.[1–8] Thus, solid-state hydrogen storage still remains a scientific and technical challenge towards implementing a "Hydrogen Economy".[9,10]

With the aim of accelerating the market introduction of hydrogen and FC technologies, the Fuel Cells and Hydrogen Joint Undertaking (FCH JU)[11] launched the HYPER project in 2012.[12,13] The three-year project aimed to develop and demonstrate a market-ready, portable power pack comprising of an integrated and cost effective modular polyelectrolyte membrane FC (PEM FC) and a hydrogen storage system, readily customised for application across multiple low power markets from the 20 W_e to 500 W_e scale, such as power tool charging, emergency lighting, security and remote monitoring.[12,14] Technical barriers such as increasing FC power output, and reducing the size and weight of hydrogen storage modules have thus far prevented exploitation of this market. Moreover, manufacturing economies of scale are difficult to realise as end user applications have very diverse requirements.[12] The HYPER project was conceived to address these challenges through the development of a scalable and flexible portable power pack.

The key components of the proposed HYPER portable power pack were originally: (1) a core FC based on 50 W_e modules which could be assembled to provide an electrical output of up to 500 W_e, (2) a common interface (hydrogen supply and control electronics) to use with alternative hydrogen supply modules to meet the needs of a range of end user applications, (3) a light-weight, protective casing incorporating user control and display panels and (4) a hydrogen storage module. One novel aspect of HYPER was the implementation of two generic types of (interchangeable) hydrogen storage modules; gaseous and solid-state (Figure 1). One of the main technical challenges of HYPER was to develop a suitable solid-state store based on nanostructured advanced hydride materials that would be compatible with the PEM FC. The material-based targets are summarized in Table 1. One of the of potential solutions was based on Ammonia Borane (NH_3BH_3, AB) as a storage material.

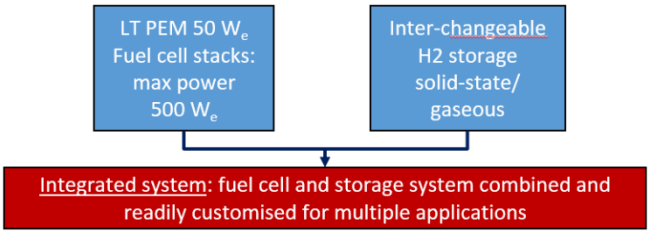

Figure 1. Schematic of proposed HYPER system [12]

[a] L., Bravo Diaz, Dr J.M., Hanlon, Professor D.H. Gregory
WestCHEM, School of Chemistry
University of Glasgow, Glasgow, G12 8QQ, UK.
E-mail: Duncan.Gregory@Glasgow.ac.uk.
[b] L., Bravo Diaz, Dr. M, Bielewski
Directorate for Energy Transport and Climate
European Commission, Joint Research Centre (JRC)
Petten, The Netherlands.
[c] Dr.A. Milewska
Department of Thermal Processes
Institute of Power Engineering
02-981 Warsaw, Poland.

Table 1: Targets for the hydrogen storage material to meet the HYPER requirements for the solid-state module.[12]

Targets for the hydrogen storage material	
H_2 gravimetric capacity / wt. %	≥ 6
H_2 volumetric capacity / g H_2 L^{-1}	30
H_2 desorption temperature / °C	≤ 250
Surface temperature / °C	≤ 80
Temperature range of H_2 delivered to the PEM FC / °C	10-30
Purity of H_2 delivered to the PEM FC / %	99.97[15]

AB has both a high H_2 gravimetric capacity (19.6 wt. %) and volumetric density (146 g H_2 L^{-1}).[16] It is solid at ambient conditions and dehydrogenates at relatively low temperatures due to the thermodynamically favourable interaction of protic $H^{\delta+}$ and hydridic $H^{\delta-}$ hydrogens that polarize the bonds and the molecule. AB decomposition follows a multistep exothermic process (Figure 2). At *ca*. 110 °C, AB melts and subsequently dehydrogenates. Two successive exothermic reactions then occur between 100 – 200 °C, before a final dehydrogenation of the polymeric material results in boron nitride (BN) formation (at too high a temperature for practical hydrogen storage).

A remarkable 13 wt. % of H_2 can be recovered from AB below 200 °C which makes AB attractive for chemical hydrogen storage and of particular interest for its application in portable power packs. [16–20] [21] However, several deleterious gaseous by-products including ammonia, diborane, monomeric aminoborane and borazine are released alongside hydrogen upon AB decomposition.[17,22,23] These species lead to poisoning and degradation of a PEMFC,[24] and so approaches to suppress these unwanted by-products must be investigated. Further, despite the unique properties of AB as a solid-state hydrogen storage material, challenges remain regarding the improvements in its kinetics,[25–28] temperature of decomposition[22] and ultimately its regeneration.[17,29,30] Various approaches have been taken to address the "on-board" technical challenges (by-products, kinetics, desorption temperature). These strategies include destabilization by: solubilisation in aprotic solvent[31,32] (e.g. ionic liquids),[33,34] additives (e.g. metal salts, metallic-based nanostructures),[35–44] chemical modification (e.g. amidoboranes)[45–52] and nanoconfinement (using an inert porous host to confine AB, e.g. silica).[53–55]

Carbon, with low weight, high abundance, low cost and low reactivity towards guest materials is an example of an effective porous host for confinement of AB. Carbon cryogels result in depressed dehydrogenation onset temperatures with the suppression of ammonia[56] while activated carbon (AC)-confined AB apparently begins to release H_2 at room temperature with one of the decomposition steps involving an acid-base reaction between the AC and the hydridic $H^{\delta-}$ in AB (which interacts with the $H^{\delta+}$ of the COO-H groups present in AC).[57] Graphene-based materials can also be applied as hosts, including graphene oxide (GO) which has enabled reversible hydrogenation of AB and release of pure hydrogen below 100 °C.[58] Further performance modifications can be made to confined AB by adding metals (e.g. Li)[59] or metal salts and [37,60] for example, graphene-supported metal chloride composites dehydrogenate from 90 °C with suppression of by-products.[61]

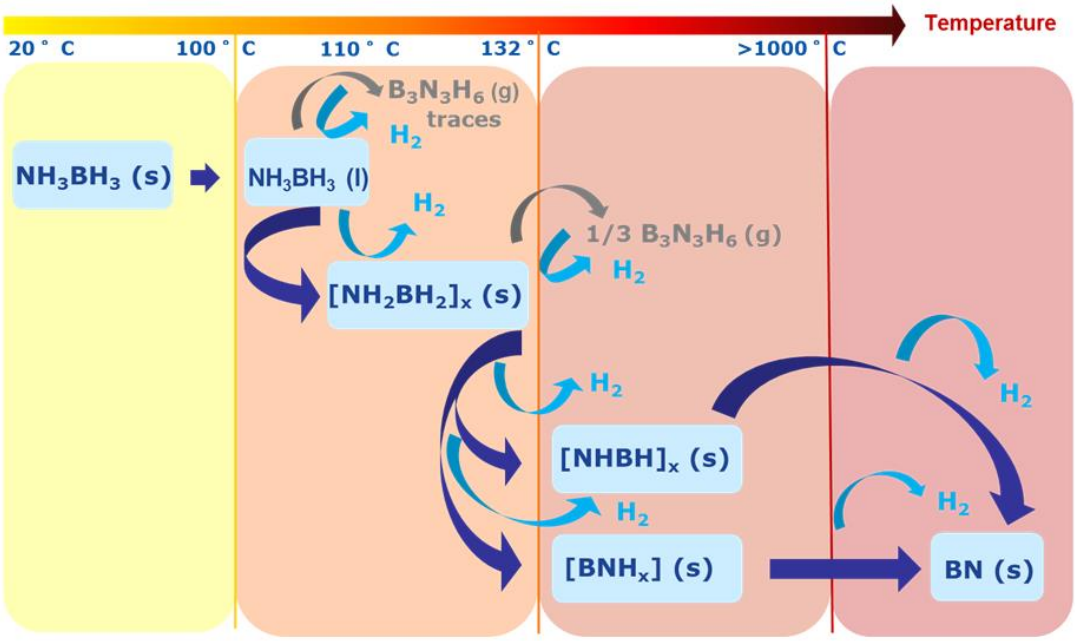

Figure 2: Schematic of the thermal decomposition of ammonia borane (NH_3BH_3, AB).

Alternatively/additionally, an "external" filter could be applied to purify the H_2 supply to the FC. For example, tetraethylene glycol dimethylether (T4EGDE) acted as a promoter and filter (combined with commercial AC) for use in a power pack with AB pellets to drive an unmanned aerial vehicle (UAV) for 57 min with fast load-following ability and rapid response time using a 200-W_e PEM FC.[21] A similar system, additionally employing catalytic amounts of palladium nanoparticles (PdBPs), powered a 200-W_e PEM FC stack for 25 min. This H_2 generator was operated autothermally without an external heater by recycling waste heat produced during AB dehydrogenation.[62]

In this paper, we discuss the first steps within the HYPER project to designing a tank that could deliver pure hydrogen to a PEMFC. No nanoconfined AB-based H_2 generator had been used in a practical application previously. This study focuses on the necessary development of nanoconfined and nanocomposite AB materials in a lab scale tank and how the system might be scaled up to fuel a PEMFC under the portable power pack working criteria. Carbon-based/AB nanocomposites provided pure hydrogen at reduced temperature with the addition of a cheap metal halide external filter. This initial investigation suggests that a working tank could be thermally managed successfully, paving the way for more sophisticated system designs.

Results and Discussion

Development and testing of solid-state hydrogen storage module materials

AB-based composites were developed using carbonaceous materials with a view to demonstrating their applicability as stores in the HYPER portable power pack. Several types of highly ordered mesoporous carbons, activated carbons (AC), and graphene (G) were employed either to prepare physically mixed nanocomposites (*via* ball milling) or to be used as inert matrices for AB nanoconfinement purposes (*via* solution impregnation). Full discussion of the materials characterisation, reaction pathways and mechanisms will be reported elsewhere but Table 2 summarizes the thermal behaviour of a selection of the composites prepared as compared to as-received AB.

An onset temperature of 112 °C and a dehydrogenation peak temperature of 125 °C were observed for as-received AB from DTA analysis (Figure 3). The DTA curve illustrates the characteristic multi-step decomposition of AB in the range from RT - 160 °C with an endothermic peak corresponding to the melting of AB at 115 °C and subsequent exothermic decomposition. The TG curve gave a corresponding weight loss of 65.6 wt. %; much higher than the expected H_2 weight loss of 13.4 wt. % in the range of temperatures studied. This difference in the weight loss can be rationalised in terms of the release of other gaseous by-products besides hydrogen and indeed the evolved gas analysis by mass spectrometry confirmed this. The species corresponding to each mass ratio were assigned according to the products of the thermolytic decomposition of AB described in the literature. [22,23] Peaks were accordingly detected for m/z=17, assigned to ammonia (NH_3); m/z=13 and m/z=27 corresponding to the known mass spectrum of diborane (B_2H_6);[63] m/z=28 and m/z=29 assigned to BNH_x species; m/z=29 corresponding to the mass spectrum of monomeric aminoborane (BH_2NH_2)[22] and m/z=80 consistent with borazine ($(BHNH)_3$).[64] These by-products would be detrimental for the PEM FC, dramatically decreasing the performance and longevity of the fuel cell.

From the materials shown in Table 2, the lowest dehydrogenation temperature was obtained for the *m-AB/AC* composite (sample 2) prepared by high energy ball milling of AB and AC (AB:AC = 40:60, wt.%). No endothermic melting process was observed in the DTA profile upon thermal decomposition of this sample and both the dehydrogenation onset temperature and peak temperature for the first release were reduced compared to AB itself. Thus, simple physical mixing by ball milling appears to be encouraging in terms of improving dehydrogenation temperatures and this would be a relatively easy process to scale-up. However, the high weight loss in the TGA profile suggests the release of unwanted by-products and in fact, traces of diborane, monomeric aminoborane and borazine were detected in the outgas by MS. Therefore, despite reducing dehydrogenation temperatures, the release of by-products, even if at a lower level than AB itself, renders this composite unsuitable for use with a PEM FC.

Table 2. Selected thermal decomposition parameters for AB-Carbon composites from TG-DTA-MS.

Sample	Identifier	Carbon host	AB:C ratio / wt.%	Preparation	T_{onset} / °C	T_{peak} / °C	Mass loss / wt.%	Mass loss of H_2 / wt.%	Gases evolved
1	*AB*	-	100:0	-	112	125	65.6	13.4	H_2, B_2H_6, BH_2NH_2, $(BHNH)_3$, NH_3
2	*m-AB/AC*	AC	40:60	ball milling	85	104	28.1	5.4	H_2, B_2H_6, BH_2NH_2, $(BHNH)_3$, NH_3
3	*s-AB/AC*	AC	40:60	solution-impregnation	96	112	5.9	5.4	H_2, NH_3
4	*m-AB/G*	G	33:67	ball milling	95	113	16.1	4.5	H_2, B_2H_6, BH_2NH_2, $(BHNH)_3$, NH_3

The most promising material of those in Table 2 in terms of product selectivity was the *s-AB/AC* composite (sample 3) prepared by the solution-impregnation process (AB:AC = 40:60, wt%). As for *m-AB/AC*, this composite showed an improved dehydrogenation performance by comparison to as-received AB. The DTA curves of as-received AB and the *s-AB/AC* composite are presented in Figure 3, in which it is possible to observe the remarkable contrasts in their thermal behaviour. The endothermic melting of AB (115 ˚C) followed by the first exothermic dehydrogenation step at 125 ˚C are clear in the DTA profile of as-received AB. By contrast, the *s-AB/AC* composite exhibits no discernible melting transition and yields only an exothermic peak at 112 ˚C, associated with hydrogen release.

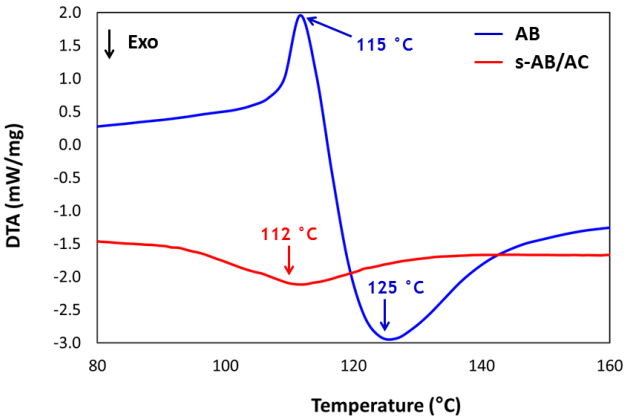

Figure 3. DTA profiles of AB and the *s-AB/AC* composite from RT - 160 ˚C at a heating rate of 5 ˚C min^{-1}.

The most important aspect of the *s-AB/AC* composite when compared to as-received AB is the suppression of borazine upon thermal decomposition. From MS measurements, hydrogen was released as the major product and the release of other by-products was rendered negligible (undetectable) with only traces of ammonia (NH_3) observed besides hydrogen. The *s-AB/AC* composite starts to release hydrogen at lower temperatures than AB although inevitably the amount released is reduced (5.4 wt.%) compared to AB itself (13.4 wt.%) give that the composite contains 60 wt.% AC (AB:AC = 40:60, wt%). Given that no boron-containing gaseous species were detected for *s-AB/AC*, the implication was that if the NH_3 release could be suppressed, then nominally pure hydrogen would become available to the PEM FC. The strategy proposed for ammonia removal is the introduction of a purification system, a $NiCl_2$ filter, which is discussed below.

That borazine release was suppressed whereas ammonia release was observed provides some indications of the nature of the nanocomposites and of the nanoconfinement of AB in the solution impregnated material. One possible effect of nanoconfinement is to induce destabilization of the -BH_3 group in AB, perturbing the intermolecular N-H···H-B network. Similar enhanced dehydrogenation of AB in CMK-3, an ordered mesoporous carbon, also led to borazine suppression (with ammonia the only other gas released).[59] In this case, the destabilisation of AB was proposed to derive from acid-base reactions between the $H^{\delta-}$ in the AB -BH_3 group and $H^{\delta+}$ from O-H and COO-H groups on the surface of the carbon host. A similar destabilisation mechanism was proposed for AB confined in an activated carbon composite, although this composite was unstable under ambient conditions.[57]

Hydrogen purification system

Despite achieving decomposition product selectivity in *s-AB/AC* and excluding boron-based by-products, the release of gaseous ammonia, even in trace amounts, could damage the PEM fuel cell. Therefore, the use of an external filter that could absorb ammonia (and potentially other by-products) was proposed to maximise the hydrogen purity of the system.[12]

Metal halide salts were investigated as potential filter materials for the selected *s-AB/AC* composite, with $NiCl_2$ as a focus. $NiCl_2$ coordinates ammonia to form the hexamine $Ni(NH_3)_6Cl_2$. It can theoretically store 44.1 wt. % ammonia.[65,66] There are also previous reports that doping AB with nickel can reduce by-product release (such as borazine) during thermal decomposition and that graphene-supported nickel chloride nanoparticles were highly efficient catalysts for AB dehydrogenation. [60,61] In the latter case, composites demonstrated improvements in dehydrogenation and a negligible release of by-products (ammonia, diborane and borazine). $NiCl_2$ is therefore interesting from an application point of view as it could serve a dual purpose, sequestering both ammonia and boron-based by-products.

Preliminary experiments in which an AB composite was mixed directly with $NiCl_2$ and heated demonstrated ammonia absorption by the halides. Subsequent investigations were performed using an external filter set-up (containing 1 g of $NiCl_2$) placed downstream from the AB composite store connected to a Hiden volumetric instrument coupled with MS to characterise the outgas (see Experimental Section).

The *m-AB/G* composite (AB:G = 33:67 wt.%) had been previously shown in the decomposition experiments to be the least promising material in terms of by-products release (i.e. it released the least pure hydrogen; Table 2). For this reason, at the outset, it was considered the best material to test the efficacy of the $NiCl_2$ filter against by-products release. Figure 4 shows the MS profiles from the evolved gas stream for *m-AB/G*, comparing the gases released upon thermal decomposition with and without the use of the $NiCl_2$ filter. The MS profiles were recorded from RT - 200 ˚C at 5 ˚C min^{-1}. Figure 4a-d illustrate that the $NiCl_2$ filter reduces all the evolved gaseous boron species compared to the unfiltered material, whereas evolved ammonia was completely captured by the filter (Fig 4e). These results, therefore, illustrate the efficacy of $NiCl_2$ as a filter.

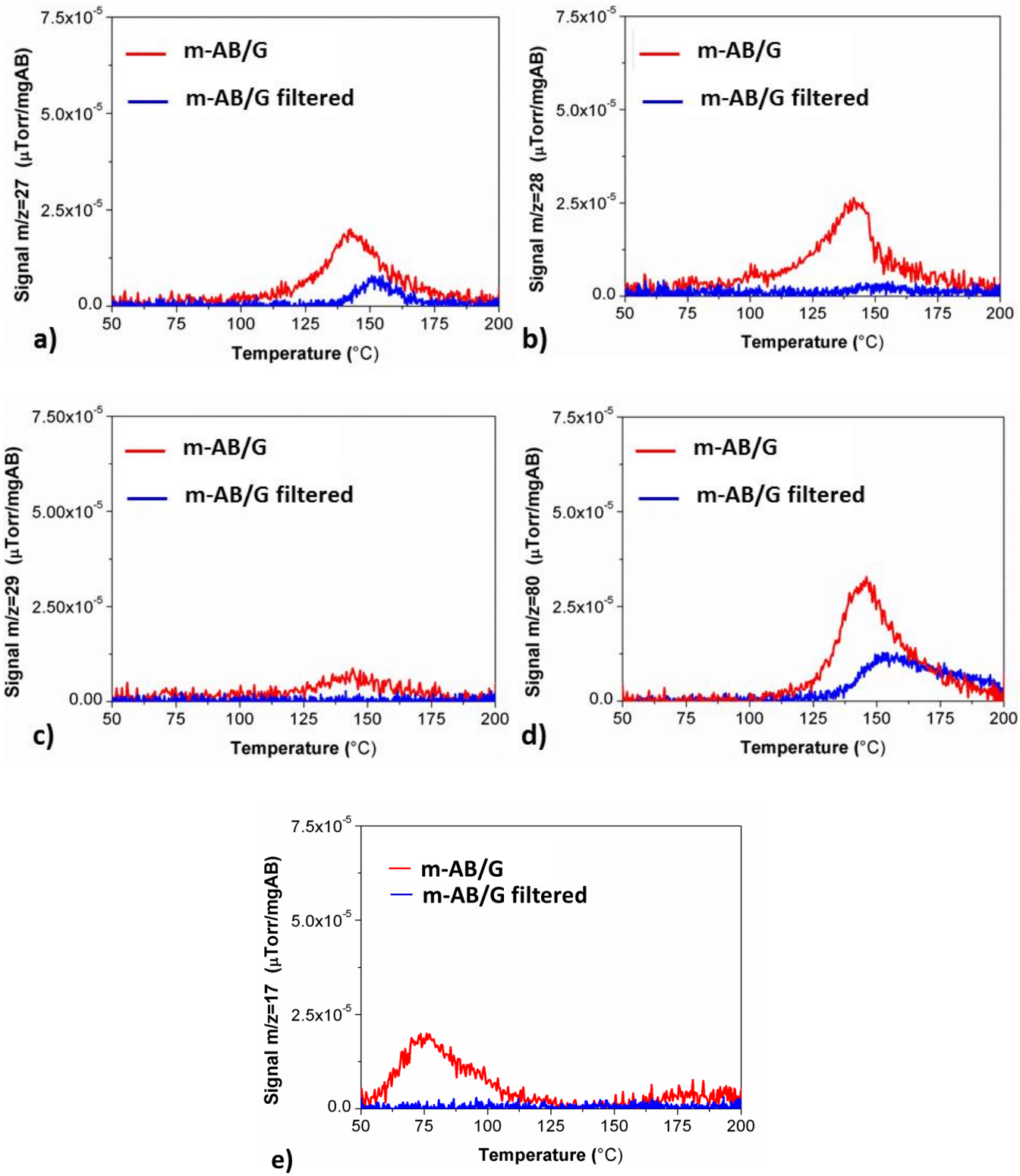

Figure 4. Comparison of MS profiles of the *m-AB/G* composite with/without the use of an $NiCl_2$ filter recording: (a) diborane evolution (m/z=27); (b) BNH_x species evolution (m/z=28); (c) BNH_x species evolution (m/z=29); (d) borazine evolution (m/z=80); (e) ammonia evolution (m/z=17).

Following the positive observations noted from the *m-AB/G* sample, equivalent experiments were run on the best-performing composite, *s-AB/AC*. Figure 5a shows the MS profiles of all the expected gases released upon thermal decomposition of *s-AB/AC* with the use of the $NiCl_2$ filter, while Figure 5b presents an expanded MS plot for ammonia (m/z=17) with and without the use of the $NiCl_2$ filter. Hydrogen dominated the mass spectra as expected and the concentration of all by-products was negligible within the MS detection limit (MS sensitivity of 100 ppb). Most importantly, unlike "unfiltered" *s-AB/AC*, no trace of ammonia was detected in the mass spectra and it could be assumed that the gas was trapped by the $NiCl_2$ filter, ensuring high H_2 purity. Hence, by combining the selective desorption properties of *s-AB/AC* with a $NiCl_2$ filter, hydrogen becomes the only detectable evolved gas and its purity is considered extremely likely to meet the requirements of the fuel cell (99.97%).[15]

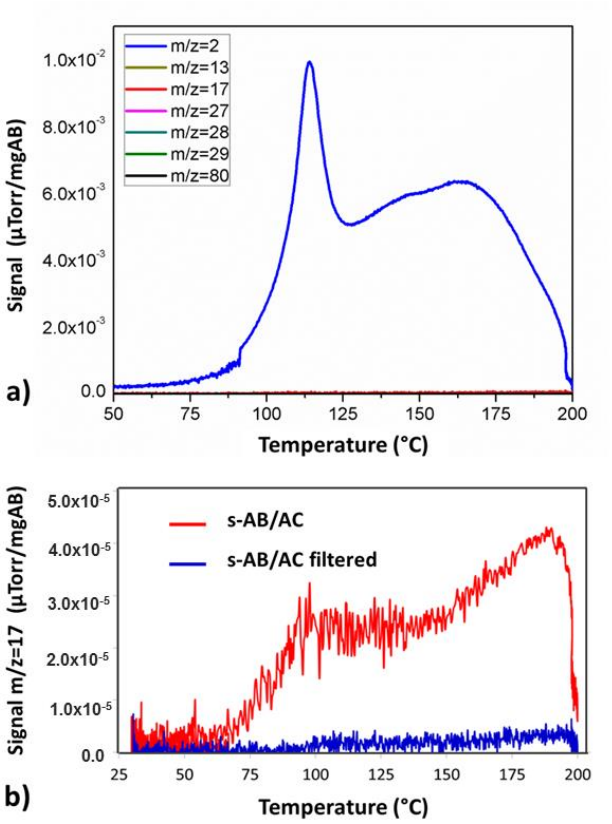

Figure 5. Evolved gas mass spectra for: (a) all thermal decomposition products from *s-AB/AC*, employing $NiCl_2$ as a filter; (b) ammonia (m/z=17) released during the decomposition of the *s-AB/AC* composite both with and without the use of the $NiCl_2$ filter. All spectra were recorded for *s-AB/AC* heated at 5 ˚C min^{-1} from RT - 200 ˚C.

Hence, the composites prepared from AB and activated carbon (*m-AB/AC*, *s-AB/AC*) outperform AB itself and AB/graphene composites (*m-AB/G*) in terms of dehydrogenation temperature and gravimetric capacity. The latter parameter reflects the reduction in gaseous by-products in the AC composites and these can be minimised by solution impregnation of the active material (AB) in the AC matrix (*s-AB/AC*). Combined with an $NiCl_2$ filter, all trace of deleterious gases can be removed from the fuel supply. The enhanced dehydrogenation temperature (T_{onset} of 96 °C), high H_2 gravimetric density (≈6 wt %) and high purity of delivered hydrogen ensure that this material would be the most promising of those investigated as a candidate for a solid-state storage module in a portable power pack.

Simulations of a storage tank with AB-based material

The objective of this modelling study was a preliminary exploration of the behaviour of an ammonia borane (AB) based composite material, in which AB is combined with a nanostructured carbon matrix. A numerical model of an AB-based storage tank was prepared based on literature data and the available experimental results.

Firstly, a kinetic model of reaction rate was selected. The decomposition of neat AB has previously been described by Choi *et al*. as a nucleation and growth reaction.[67] This model was employed as the basis of the simulations after successful validation of the kinetics through theoretical and experimental measurements. The validation experiments were performed using the *m-AB/AC* sample based on the availability of data and its relatively good performance. The kinetic parameters used for the AB simulations, the validation experiments considered, and the computational mesh of the tank used for the simulations are presented in the Experimental Section. The model, once successfully validated, was used for further simulations. However, it must be emphasised that ideally the number of experimental measurements should be higher in order to eliminate model uncertainties at lower temperatures.

Initiation simulations were subsequently performed using a numerical model implemented in the Matlab software package. These one-dimension simulations were made to investigate the influence of the initiation temperature on the decomposition reaction rate. The AB-based material needs to be heated to an onset temperature of 95 °C. It was assumed that the storage tank would be working in batch mode and a glow plug could initiate the process by rapidly increasing the temperature above the onset level. The glow plug is a heating device with a tip that reaches temperatures of up to 1000 °C in less than 5 seconds.[68] The maximum temperature considered from the glow plug was 800 °C. It was observed from the 1D simulations that the decomposition reaction started 25 s after initiation and that the reaction propagation front progressed at almost constant speed (Figure 6). However, some delay was observed during the 1st step of the reaction (Figure 6c), originating from the time-dependence of the reaction rate. The model assumes that the elevated temperature can induce the reaction over a period long enough for unreacted substrate to remain available in the system. However, such material behaviour has not yet been tested experimentally and the results should be interpreted cautiously.

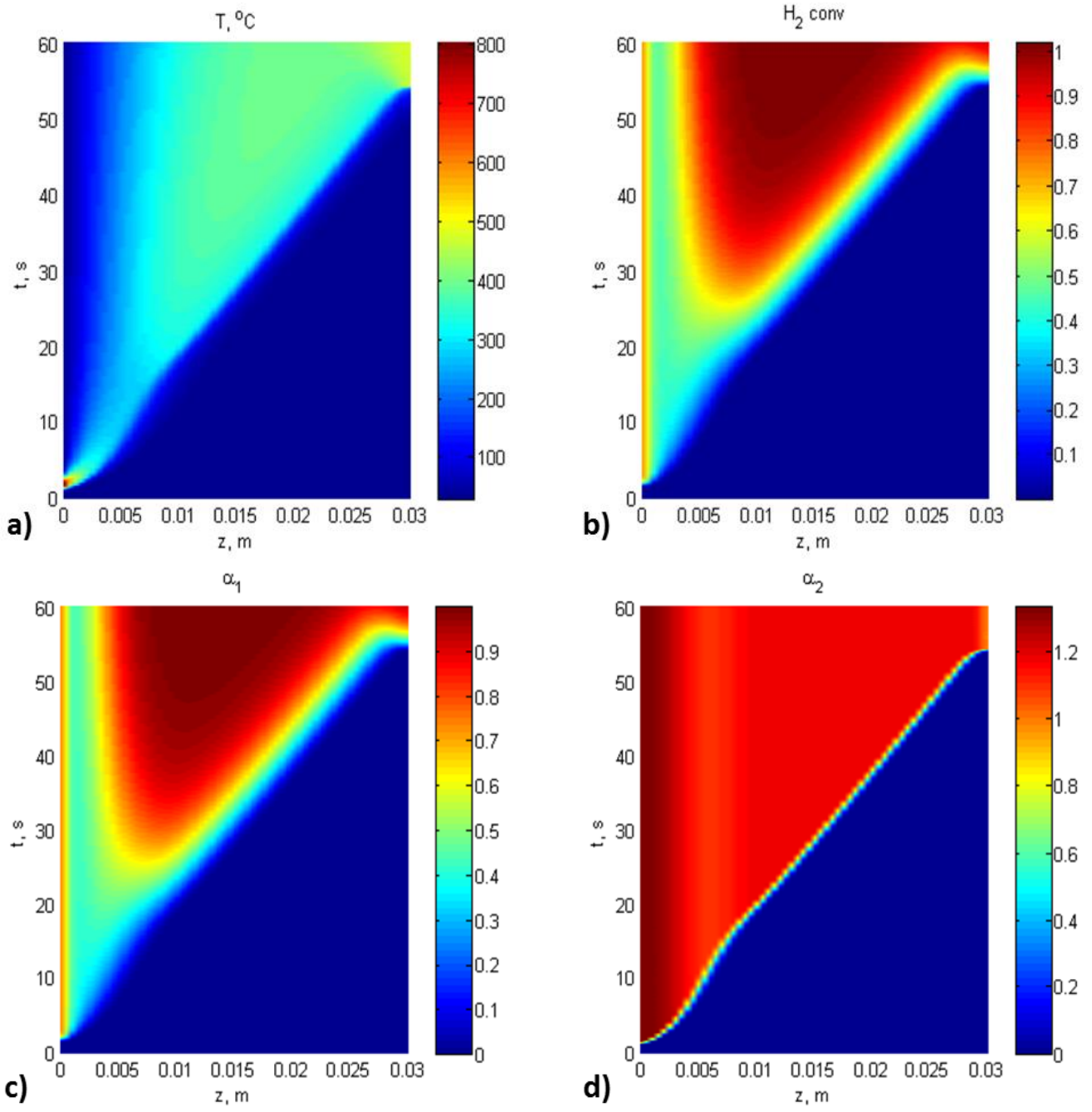

Figure 6. Simulations results for the 1D model of the *m-AB/AC* material showing: (a) material temperature; (b) total conversion of hydrogen from AB; (c) conversion in the 1st reaction step; d) conversion in the 2nd reaction step.

Finally, tank model simulations were developed using a CFD (Computational Fluid Dynamics) model generated by Ansys Fluent software. The main aim of the simulations was to check if the glow plug could initiate *m-AB/AC* dehydrogenation. The numerical model of the tank and further specifications are presented in the Experimental section. For the simulations, it was assumed that the total volume of the tank was filled with the AB-based material. The reaction rate was limited by the heat transfer inside the material and the glow plug was installed at the base of the tank. The maximum temperature was achieved after 5 s, maintained for 180 s and then cooled to 20 °C, over 60 s. The outer wall of the tank was not modelled in detail but was included in simulations as the shell, with conduction based on steel material of 6 mm thickness.

The series of simulations were made for two maximal temperatures for the glow plug: 500 °C and 800 °C. The temperature and reaction conversion inside the tank was monitored for both conditions. The volume-averaged temperature is presented in Figure 7. The highest temperature was reached with the lower initiation temperature (500 °C). This was caused by a longer initiation period for the nucleation reaction, which led to an accumulation of unreacted intermediate products. When the local temperature reached the onset value, the reaction rate rapidly increased after the relatively long nucleation period. In principle, this could lead to thermal runaway and further stability tests of AB-based materials under these conditions are therefore necessary. Conversely, when the initiation temperature was 800 °C the reaction proceeded more quickly. The growth phase started following a shorter nucleation period and unlike the 500 °C case, unreacted intermediate products were not accumulated in the tank.

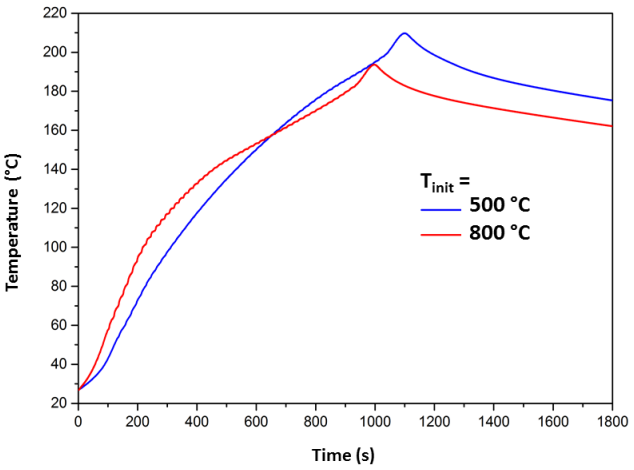

Figure 7. Volume-averaged temperature of the *m-AB/AC* material for different maximal initiation temperatures.

Figure 8 presents both the total reaction conversion and the conversion for each step (nucleation and growth) as a function of time. The rate of hydrogen release was almost constant in all cases. The tank was emptied after 15 minutes (900 s) when the higher initiation temperature (800 °C) is applied compared to approximately 18 minutes (1080 s) for the case of the lower initiation temperature (500 °C). Each step of the reaction is almost a linear function of time, which would suggest that the nucleation phase is the reaction step that determines the total reaction rate.

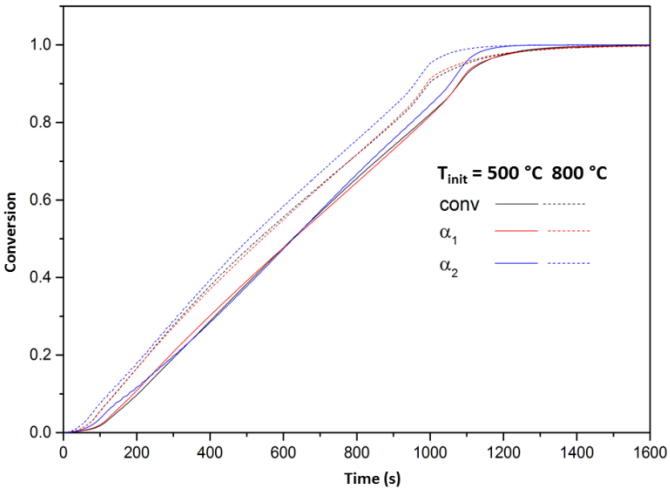

Figure 8. Volume-averaged total conversion and conversion at each reaction step for different maximal initiation temperature.

The profiles of temperature and the reaction conversion inside the storage tank are presented at selected time steps in Figure 9. After 20 s from the glow plug initiation, there was only a local increase of temperature observed in both cases. After 140 s, while the plug was still active, the bottom part of the tank was heated above the onset temperature. All hydrogen from this lower section of the tank was released in the case of the higher initial temperature (800 °C; Figure 9d). However, in the lower initiation temperature case (500 °C), the nucleation phase of the reaction was incomplete and not all the H_2 was released (Figure 9b). In the latter case, after 300 s the local temperature at the reaction front rapidly increased (Figure 9a) which in turn led to an increase in the volume-averaged temperature. At the higher initiation temperature of 800 °C, the temperature and reaction front moved almost piston-like at constant speed (Figure 9c). When the initiation temperature is 500 °C, the local reaction rate slowed and then the temperature rapidly increased. As noted above, this can lead to local overheating of the material. It should also be noted that the simulation results were very sensitive to physical properties of the material such as density, thermal conductivity and specific heat. Each of these parameters should ultimately be verified experimentally for a given composite composition (i.e. ratio of AB and selected carbon material).

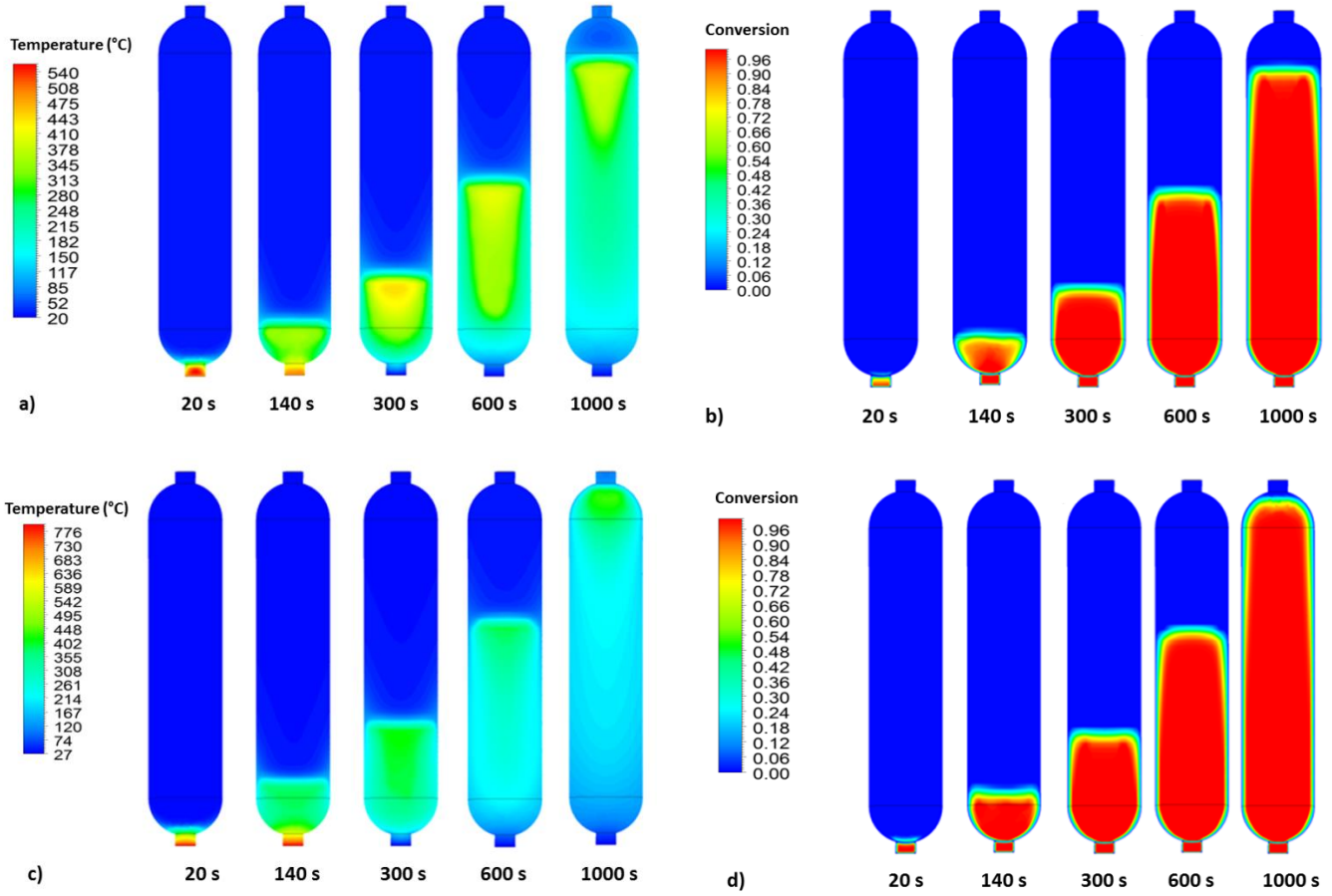

Figure 9: Temperature and conversion of hydrogen respectively for the *m-AB/AC* composite-filled tank with a maximal initiation temperature of (a, b) 500 °C; (c, d) 800 °C.

Conclusions

Ammonia borane, AB, was selected as a possible component of a solid-state hydrogen store of a portable power pack under the European FCH JU HYPER project. Despite an advantageous gravimetric content and hydrogen release temperature, gaseous by-products released on thermal decomposition would lead to irreversible damage to the PEM fuel cell component of the power pack and so strategies to suppress the release of these by-products would be essential for successful AB implementation.

Activated carbons (AC) and graphene were employed to prepare AB-based nanocomposites (*via* ball milling) and used as inert matrices for AB nanoconfinement (*via* solution impregnation) in different ratios. A selection of these were evaluated and from the results obtained, a composite with 40:60 wt. % AB:AC prepared by solution-impregnation was found to have the best overall performance with a dehydrogenation onset temperature of 96 °C and a gravimetric density of *ca.* 6 wt. % H_2 while releasing no boron-containing gases on decomposition. Remaining traces of ammonia could be completely eradicated from the fuel supply *via* the use of an external $NiCl_2$ filter, which, if necessary, could also decrease the concentration of other unwanted by-products such as diborane. No by-products were detected to within 100 ppb when using the composite coupled to a $NiCl_2$ filter.

A preliminary simulation of a storage tank based on an AB-AC composite was performed drawing on literature and experimental data. A kinetic model of the thermal decomposition based on the Avrami model of nucleation and growth[67] was successfully validated, although further experimental data will be necessary, especially at lower temperature to refine the model. 1D and 3D simulations employing the kinetic model investigated the influence of the initiation temperature on the reaction rate, showing that the reaction front moved at almost constant speed although the 1st reaction step exhibits a strong rate dependence on time. The initiation temperature of the decomposition proved crucial; at 500 °C unreacted intermediate products led to high

temperatures and local overheating of the material, whereas at 800 °C the nucleation step of reaction is abbreviated, the accumulation of unreacted material is avoided and the temperature can be regulated. Both simulation scenarios nevertheless suggest that an AB-AC tank is an extremely promising possibility given the constant rate of H_2 release. However, only with further experimental characterisation and testing will it be possible to obtain the verified requisite material properties and an improved reaction kinetics model to enable more accurate modelling of the storage tank.

Experimental

Synthesis and characterisation of solid-state hydrogen storage module materials

Materials:
Ammonia Borane (Sigma, 97%) was used as received. Activated Carbon (Sigma, 300 mesh) and Graphene nanoplatelets (Alfa Aesar, graphene nanoplatelets aggregates, sub-micron particles, S.A. 500 m^2g^{-1}) were dried under high vacuum at 400 °C overnight. This was to ensure the pores are free of oxygen and water before sample preparation.

Synthesis:
High energy ball milling was used to prepare composites containing activated carbon (*m-AB/AC*) and graphene (*m-AB/G*).For the *m-AB/AC* composite, 320 mg of Ammonia borane (AB) and 480 mg of activated carbon (AC) were ball milled for one hour using a Retsch PM 100 planetary ball mill. A ball to powder ratio of 40:1 was employed. For the *m-AB/G* composite 200 mg of AB and 400 mg of graphene were ball milled using the same parameters. The remaining AB-AC composite (*s-AB/AC*) was prepared by solution-impregnation. For the *s-AB/AC* composite, 120 mg of AB and 180 mg of AC were added to a 50 ml Schlenk flask and 5-10 ml of THF (Sigma, >99.9%, inhibitor free) added. The mixture was then stirred for 1 h followed by drying under vacuum using a Schlenk line with liquid N_2 used as a solvent trap. The process was repeated extending the drying time of > 72 hours with the liquid N_2 trap removed after 1 h of drying. All sample preparations were undertaken inside an N_2 (g) recirculating glove box (Saffron Scientific, H_2O, O_2 < 1 ppm).

Thermal decomposition:
Thermal analysis (Thermogravimetric-Differential Thermal Analysis-Mass Spectrometry; TG-DTA-MS) was performed using a Netzsch STA 409 analyser interfaced to a Hiden HPR 20 Mass Spectrometer. The STA analyser was located within an Argon-filled MBraun UniLab glove box (< 0.1 ppm H_2O, 0.1 ppm O_2). Approximately 5 mg of each AB composite were heated to 200 °C in an alumina pan under flowing Ar at a heating rate of 5 °C min^{-1} and held at 200 °C for 30 min.

Hydrogen purification system measurements

Nickel Chloride (Sigma, 98 %) was investigated as potential filter material. Experiments were performed using an external filter set-up (containing 1 g of filter material) with a Hiden Isochema HTP1-S Volumetric Analyser coupled to a QIC-20 Mass Spectrometer (MS) (Figure 10). The location and configuration of the filter downstream ensures that gas which is released from the AB sample flows through the absorbing material. The composition of the gases evolved from the composites as a function of temperature (and time) was determined by temperature programmed decomposition (TPD) measurements from room temperature (RT) to 200 °C at a heating rate of 5 °C min^{-1}. Helium was used as a carrier gas. The helium gas flow was fixed at 30 ml min^{-1} and the measurement was performed at atmospheric pressure.

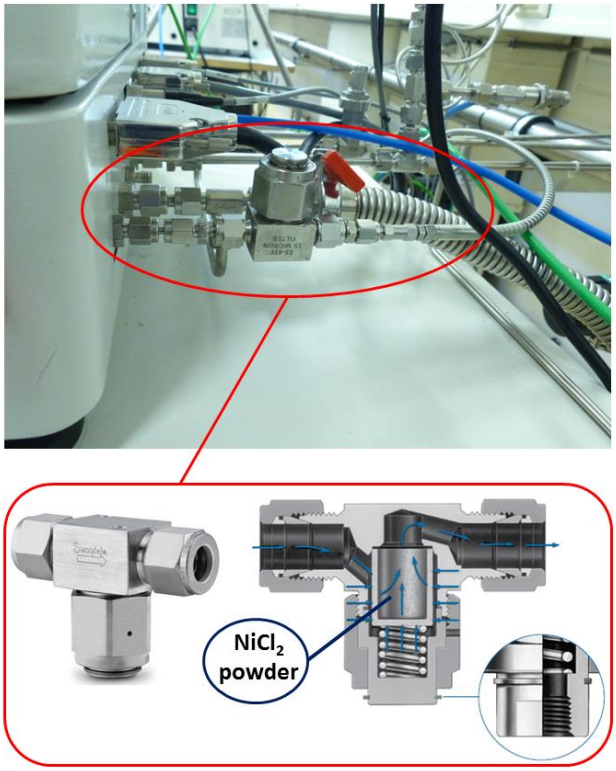

Figure 10. Design of the external filter and its location for by-product gas release testing. The filter is located at the inlet of the capillary that connects the volumetric instrument to the MS.

Simulations of a storage tank with AB-based material
Numerical simulations have been performed taking into account the mechanism for hydrogen release in ammonia borane. Thermally-induced dehydrogenation of AB occurs in 3 steps which are presented in Table 3.[69] Reaction steps 1 and 2 release hydrogen over the range of temperatures studied and are relevant for PEM fuel cells.

Table 3. Reaction steps of AB decomposition.[69]

Reaction step	Reaction	Mass of H_2 / wt. %	Temperature / °C	Enthalpy / kJ mol^{-1} H_2
1	$NH_3BH_3 \rightarrow 1/x\ (NH_2BH_2)_x + H_2$	6.5	90-117	-22
2	$1/x\ (NH_2BH_2)_x \rightarrow 1/x\ (NHBH)_x + H_2$	6.5	150-170	-15
3	$1/x\ (NHBH)_x \rightarrow 1/x\ (BN)_x + H_2$	6.5	> 500	-

The AB decomposition is a nucleation and growth reaction and can be described by Avrami equations. Choi *et al*. have previously presented a kinetic model for the decomposition of AB which was used as the basis for the simulations.[67]

$$\frac{d\chi}{dt} = \chi_1 \frac{d\alpha_1}{dt} + \chi_2 \left[\alpha_2 \frac{d\alpha_1}{dt} + \alpha_1 \frac{d\alpha_2}{dt}\right]$$

where

$$\frac{d\alpha_i}{dt} = n_1 k_i^{n_i} t^{n_i - 1}(1 - \alpha_i)$$

and χ_1 and χ_2 are the molar equivalents of H_2 released in the 1st and 2nd step of the reaction (Table 3), α1 and α2 are the conversion ratios for each step and k_i are the Arrhenius kinetic constants.

The model assumes that the reaction rate is a function of temperature, conversion and time. The kinetic model was fitted based on available experimental data and literature data.[67] The kinetics parameters were calculated using a Levenberg–Marquardt algorithm implemented in the Matlab software package.

The proposed kinetic model was validated only for temperatures above 100 °C. However, the initiation phase of the reaction is very important for correct simulation of the whole storage tank. Thus, the above model, after some correction (Table 4), was successfully validated for ramped-temperature experiments. The 3 experiments from the literature[67] and one experiment on *m-AB/AC* described herein were used for the validation of the obtained kinetic parameters.

Table 4: Kinetic parameters for the kinetic model of thermal decomposition of *m-AB/AC*

	1st step	2nd step
χ_i	0.6	1.9
α_i	1.0×10^2	2.7×10^{14}
E_{ai} / J mol^{-1}	3.4×10^4	1.3×10^5
n_i	1	0.5
ΔH / J mol^{-1}	-2.2×10^4	-1.5×10^4

A comparison of the calculated and experimental results is presented in Figure 11. The successfully validated model was therefore used for the simulations. However, it must be emphasised that the number of experimental measurements should be higher to eliminate model uncertainties at lower temperatures.

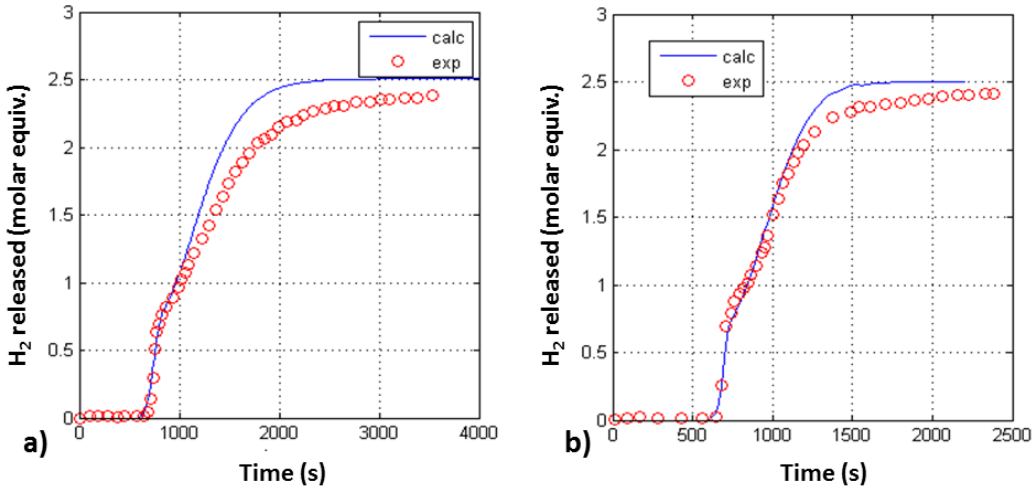

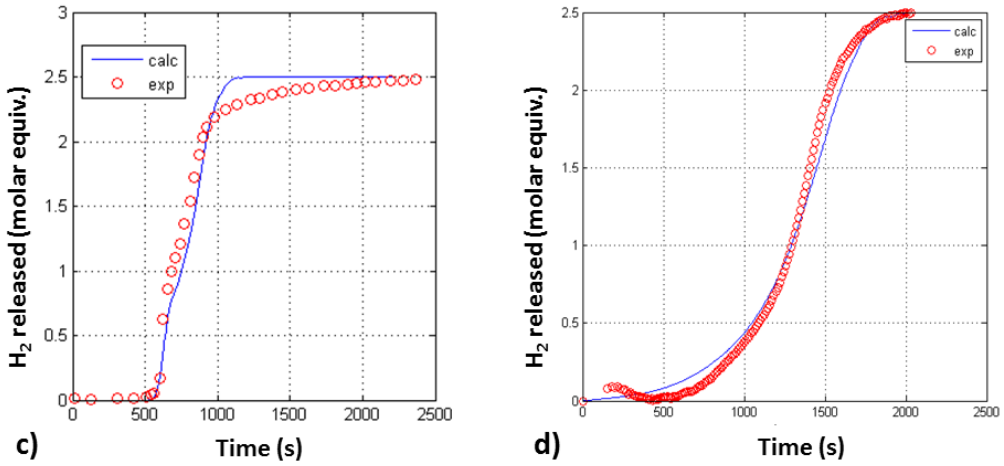

Figure 11. Comparison of the experimental measurements and simulation results for ramped-temperature conditions: a) 160 °C, b) 200 °C, c) 250 °C, d) 200 °C. Data for (a)-(c) were taken from reference [67]. Data for (d) were taken from experiment results for *m-AB/AC* presented herein.

The 3D simulation of the performance of the *m-AB/AC* composite was performed using a tank based on a storage tank supplied by Swagelok, model *316L*, with a volume of 0.16 L and a maximum operating pressure of 300 bar. To initiate the dehydrogenation of the composite, a glow plug would be used, which was located at the bottom of the tank. The maximum temperature of the glow plug is achieved after 5 s and maintained for three minutes before a 20 s cooling period in the simulations. The conduction of the tank is based on a 6 mm thick steel material. The geometry and computational mesh of the tank model is presented in Figure 12.

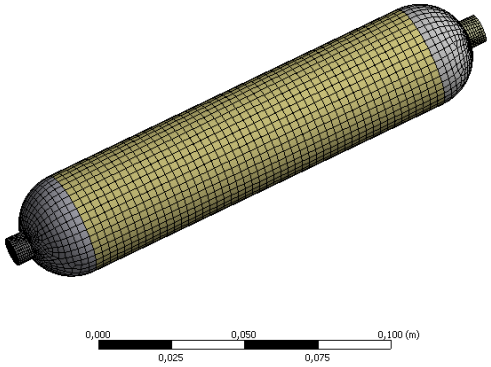

Figure 12. Geometry and computational mesh for the storage tank model.

Acknowledgements

The authors would like to thank the European Commission and the University of Glasgow for a studentship for LDB. The research post for JMH has received funding from the European Union's Seventh Framework Programme (FP7/2007-2013) for the Fuel Cells and Hydrogen Joint Technology Initiative under Grant Agreement number 303447. Associated research received funding from the European Union's Seventh Framework 610 Programme (FP7/2007-2013) for the Fuel Cells and Hydrogen Joint Technology Initiative under Grant 611 Agreement number 303447.

Keywords: Ammonia borane • hydrogen storage • polyelectrolyte membrane fuel cell (PEM FC) • ammonia • activated carbon

References

[1] L. Schlapbach, A. Züttel, *Nature* **2001**, *414*, 353–358.
[2] W. Grochala, P. P. Edwards, *Chem. Rev.* **2004**, *104*, 1283–1315.
[3] S.-I. Orimo, Y. Nakamori, J. R. Eliseo, A. Züttel, C. M. Jensen, *Chem. Rev.* **2007**, *107*, 4111–4132.
[4] T. K. Mandal, D. H. Gregory, *Annu. Reports Sect. "A" (Inorganic Chem.* **2009**, *105*, 21–54.
[5] T. K. Mandal, D. H. Gregory, *Proc. Inst. Mech. Eng. Part C J. Mech. Eng. Sci.* **2010**, *224*, 539–558.
[6] H. Reardon, J. M. Hanlon, R. W. Hughes, A. Godula-Jopek, T. K. Mandal, D. H. Gregory, *Energy Environ. Sci.* **2012**, *5*, 5951–5979.
[7] J. M. Hanlon, H. Reardon, N. Tapia-Ruiz, D. H. Gregory, *Aust. J. Chem.* **2012**, *65*, 656–671.
[8] "Technical System Targets: Onboard Hydrogen Storage for Light-Duty Fuel Cell Vehicles," can be found under https://energy.gov/sites/prod/files/2017/05/f34/fcto_targets_onboard_hydro_storage_explanation.pdf, accessed (19-08-2017).
[9] A. Züttel, A. Borgschulte, L. Schlapbach, *Hydrogen as a Future Energy Carrier*, Wiley-VCH, **2008**.
[10] N. Armaroli, V. Balzani, *ChemSusChem* **2011**, *4*, 21–36.

[11] "Fuel Cell and Hydrogen Joint Undertaking (FCH JU) projects," can be found under http://www.fch.europa.eu/, accessed (18-08-2017).

[12] "Integrated hydrogen power packs for portable and other autonomous applications (HYPER). The research leading to these results has received funding from the European Union's Seventh Framework Programme (FP7/2007-2013) for the Fuel Cells and Hydrogen Joint," can be found under http://www.fch.europa.eu/project/integrated-hydrogen-power-packs-portable-and-other-autonomous-applications, **2015**, accessed (18-08-2017).

[13] *Fuel Cells Bull.* **2012**, *2012*, 7.

[14] UK Hydrogen and Fuel Cell Association, "Markets - UK Hydrogen and Fuel Cell Association," can be found under http://www.ukhfca.co.uk/the-industry/markets/, **2014**.

[15] *ISO 14687-2:2012*

[16] U. B. Demirci, *Int. J. Hydrogen Energy* **2017**, *42*, 9978–10013.

[17] F. H. Stephens, V. Pons, R. Tom Baker, *Dalton Trans.* **2007**, *2*, 2613–2626.

[18] B. Peng, J. Chen, *Energy Environ. Sci.* **2008**, *1*, 479–483.

[19] A. Staubitz, A. P. M. Robertson, I. Manners, *Chem. Rev.* **2010**, *110*, 4079–4124.

[20] P. Wang, *Dalton Trans.* **2012**, *41*, 4296–4302.

[21] J. E. Seo, Y. Kim, Y. Kim, K. Kim, J. H. Lee, D. H. Lee, Y. Kim, S. J. Shin, D. M. Kim, S. Y. Kim, et al., *J. Power Sources* **2014**, *254*, 329–337.

[22] F. Baitalow, J. Baumann, G. Wolf, K. Jaenicke-Rößler, G. Leitner, **2002**, *391*, 159–168.

[23] M. R. Weismiller, S. Q. Wang, A. Chowdhury, S. T. Thynell, R. A. Yetter, *Thermochim. Acta* **2013**, *551*, 110–117.

[24] J. Yang, A. Sudik, C. Wolverton, D. J. Siegel, *Chem. Soc. Rev.* **2010**, *39*, 656–675.

[25] M. G. Hu, R. a. Geanangel, W. W. Wendlandt, *Thermochim. Acta* **1978**, *23*, 249–255.

[26] V. Sit, R. A. Geanangel, W. W. Wendlandt, *Thermochim. Acta* **1987**, *113*, 379–382.

[27] G. Wolf, J. Baumann, F. Baitalow, F. P. Hoffmann, *Thermochim. Acta* **2000**, *343*, 19–25.

[28] C. R. Miranda, G. Ceder, *J. Chem. Phys.* **2007**, *126*, 184703–184713.

[29] B. L. Davis, D. A. Dixon, E. B. Garner, J. C. Gordon, M. H. Matus, B. Scott, F. H. Stephens, *Angew. Chemie - Int. Ed.* **2009**, *48*, 6812–6816.

[30] A. D. Sutton, A. K. Burrell, D. A. Dixon, E. B. Garner, J. C. Gordon, T. Nakagawa, K. C. Ott, J. P. Robinson, M. Vasiliu, *Science (80-.).* **2011**, *331*, 1426–1429.

[31] J. F. Kostka, R. Schellenberg, F. Baitalow, T. Smolinka, F. Mertens, *Eur. J. Inorg. Chem.* **2012**, 49–54.

[32] W. J. Shaw, J. C. Linehan, N. K. Szymczak, D. J. Heldebrant, C. Yonker, D. M. Camaioni, R. T. Baker, T. Autrey, *Angew. Chemie - Int. Ed.* **2008**, *47*, 7493–7496.

[33] M. E. Bluhm, M. G. Bradley, R. Butterick, U. Kusari, L. G. Sneddon, *J. Am. Chem. Soc.* **2006**, *128*, 7748–7749.

[34] D. W. Himmelberger, L. R. Alden, M. E. Bluhm, L. G. Sneddon, *Inorg. Chem.* **2009**, *48*, 9883–9889.

[35] S. De Benedetto, M. Carewska, C. Cento, P. Gislon, M. Pasquali, S. Scaccia, P. P. Prosini, *Thermochim. Acta* **2006**, *441*, 184–190.

[36] S. B. Kalidindi, J. Joseph, B. R. Jagirdar, *Energy Environ. Sci.* **2009**, *2*, 1274–1276.

[37] R. Chiriac, F. Toche, U. B. Demirci, O. Krol, P. Miele, *Int. J. Hydrogen Energy* **2011**, *36*, 12955–12964.

[38] F. Toche, R. Chiriac, U. B. Demirci, P. Miele, *Int. J. Hydrogen Energy* **2012**, *37*, 6749–6755.

[39] D. J. Heldebrant, A. Karkamkar, N. J. Hess, M. Bowden, S. Rassat, Z. Feng, K. Rappe, T. Autrey, *Chem. Mater.* **2008**, *20*, 5332–5336.

[40] Y. Li, F. Fang, Y. Song, Y. Li, Q. Zhang, L. Ouyang, M. Zhu, D. Sun, *Int. J. Hydrogen Energy* **2012**, *37*, 4274–4279.

[41] T. He, J. Wang, G. Wu, H. Kim, T. Proffen, A. Wu, W. Li, T. Liu, Z. Xiong, C. Wu, et al., *Chem. - A Eur. J.* **2010**, *16*, 12814–12817.

[42] T. He, J. Wang, T. Liu, G. Wu, Z. Xiong, J. Yin, H. Chu, T. Zhang, P. Chen, *Catal. Today* **2011**, *170*, 69–75.

[43] F. Cheng, H. Ma, Y. Li, J. Chen, *Inorg. Chem.* **2007**, *46*, 788–794.

[44] D. Kumar, H. A. Mangalvedekar, S. K. Mahajan, *Mater. Renew. Sustain. Energy* **2014**, *3*, 1–7.

[45] H. V. K. Diyabalanage, R. P. Shrestha, T. A. Semelsberger, B. L. Scott, M. E. Bowden, B. L. Davis, A. K. Burrell, *Angew. Chemie - Int. Ed.* **2007**, *46*, 8995–8997.

[46] F. Leardini, J. R. Ares, J. Bodega, M. J. Valero-Pedraza, M. A. Bañares, J. F. Fernández, C. Sánchez, *J. Phys. Chem. C* **2012**, *116*, 24430–24435.

[47] Z. Xiong, C. K. Yong, G. Wu, P. Chen, W. Shaw, A. Karkamkar, T. Autrey, M. O. Jones, S. R. Johnson, P. P. Edwards, et al., *Nat. Mater.* **2008**, *7*, 138–141.

[48] H. V. K. Diyabalanage, T. Nakagawa, R. P. Shrestha, T. A. Semelsberger, B. L. Davis, B. L. Scott, A. K. Burrell, W. I. F. David, K. R. Ryan, M. O. Jones, et al., **2010**, *132*, 11836–11837.

[49] Q. Zhang, C. Tang, C. Fang, F. Fang, D. Sun, L. Ouyang, M. Zhu, **2010**, *114*, 1709–1714.

[50] H. Wu, W. Zhou, F. E. Pinkerton, M. S. Meyer, Q. Yao, S. Gadipelli, T. J. Udovic, T. Yildirim, J. J. Rush, *Chem. Commun. (Camb).* **2011**, *47*, 4102–4104.

[51] K. J. Fijalkowski, R. V. Genova, Y. Filinchuk, A. Budzianowski, M. Derzsi, T. Jaroń, P. J. Leszczyński, W. Grochala, *Dalton Trans.* **2011**, *40*, 4407–4413.

[52] G. Xia, Y. Tan, X. Chen, Z. Guo, H. Liu, X. Yu, *J. Mater. Chem. A* **2013**, *1*, 1810–1820.

[53] A. Gutowska, L. Li, Y. Shin, C. M. Wang, X. S. Li, J. C. Linehan, R. S. Smith, B. D. Kay, B. Schmid, W. Shaw, et al., *Angew. Chemie - Int. Ed.* **2005**, *44*, 3578–3582.

[54] T. Zhang, X. Yang, S. Yang, D. Li, F. Cheng, Z. Tao, J. Chen, *Phys. Chem. Chem. Phys.* **2011**, *13*, 18592–18599.

[55] S. W. Lai, H. L. Lin, T. L. Yu, L. P. Lee, B. J. Weng, *Int. J.*

Hydrogen Energy **2012**, *37*, 14393–14404.
[56] A. Feaver, S. Sepehri, P. Shamberger, A. Stowe, T. Autrey, C. Cao, **2007**, *111*, 7469–7472.
[57] G. Moussa, S. Bernard, U. B. Demirci, R. Chiriac, P. Miele, *Int. J. Hydrogen Energy* **2012**, *37*, 13437–13445.
[58] Z. Tang, H. Chen, X. Chen, L. Wu, X. Yu, *J. Am. Chem. Soc.* **2012**, *134*, 5464–5467.
[59] L. Li, X. Yao, C. Sun, A. Du, L. Cheng, Z. Zhu, C. Yu, J. Zou, S. C. Smith, P. Wang, et al., *Adv. Funct. Mater.* **2009**, *19*, 265–271.
[60] T. He, Z. Xiong, G. Wu, H. Chu, C. Wu, T. Zhang, P. Chen, *Chem. Mater.* **2009**, *21*, 2315–2318.
[61] W. Sun, H. Li, Y. Wang, *Int. J. Hydrogen Energy* **2015**, *40*, 15389–15397.
[62] S.-K. Kim, S.-A. Hong, H.-J. Son, W.-S. Han, C. W. Yoon, S. W. Nam, S. O. Kang, *J. Mater. Chem. A* **2014**, *2*, 20243–20251.
[63] "Spectrum of Diborane - NIST," can be found under http://webbook.nist.gov/cgi/cbook.cgi?ID=C19287457&Units=SI&Mask=200#Mass-Spec, accessed (19-08-2017).
[64] "Spectrum of Borazine - NIST," can be found under http://webbook.nist.gov/cgi/cbook.cgi?ID=C6569513&Units=SI&Mask=200#Mass-Spec, accessed (19-08-2017).
[65] R. Z. Sørensen, J. S. Hummelshøj, A. Klerke, J. B. Reves, T. Vegge, J. K. Nørskov, C. H. Christensen, *J. Am. Chem. Soc.* **2008**, *130*, 8660–8668.
[66] J. Breternitz, Y. E. Vilk, E. Giraud, H. Reardon, T. K. A. Hoang, A. Godula-Jopek, D. H. Gregory, *ChemSusChem* **2016**, *9*, 1312–1321.
[67] Y. J. Choi, E. C. E. Rönnebro, S. Rassat, A. Karkamkar, G. Maupin, J. Holladay, K. Simmons, K. Brooks, *Phys. Chem. Chem. Phys. Phys. Chem. Chem. Phys* **2014**, *16*, 7959–7968.
[68] "Glow plugs," can be found under http://beru.federalmogul.com/sites/default/files/ti_04_gb_2014_fm.pdf, accessed (19-08-2017).
[69] Y. Kim, Y. Kim, S. Yeo, K. Kim, K. Jung-Eun Koh, J. E. Seo, S. J. Shin, D. K. Choi, C. W. Yoon, S. W. Nam, *J. Power Sources* **2013**, *229*, 170–178.

BN_x	Borane-based species
°C	Degrees Celsius
DoE	Department of Energy
DTA	Differential thermal analysis
E_{ai} (J mol^{-1})	Energy of activation of the i step of the reaction
FCs	Fuel cells
FCH JU	Fuel Cells and Hydrogen Joint Undertaking
G	Graphene
H_2	Hydrogen
H_2 conv	Total conversion of hydrogen
$H^{\delta+}$	Protic hydrogen
H^{δ}	Hydridic hydrogen
k_i	rate constant
LT PEM membrane	Low temperature polymer electrolyte
m-	Milled
MS	Mass spectrometry
NH_3	Ammonia
NH_3BH_3	Ammonia borane
$(NH_2BH_2)_x$	Polymeric amminoborane
$Ni(NH_3)_6Cl_2$	Hexammine nickel chloride
$NiCl_2$	Nickel chloride
PdBPs	Palladium nanoparticles
PEM FC	Polymer electrolyte membrane fuel cell
ppb	Part per billion
s-	Solution-impregnated
T (°C)	Temperature
T (s)	Time
T4EGDE	Tetraethylene glycol dimethylether
TGA	Thermogravimetric analysis
TG-DT-MS	Thermogravimetric, differential thermal, mass spectrometry analyses
T_{onset}	Onset temperature
T_{peak}	Peak temperature
US	United States of America
W_e	Watt electric
Wt. %	Weight percent
Z (m)	height of the tank
χ_1	molar equivalents of H_2 released in the 1st step of the reaction
χ_2	molar equivalents of H_2 released in the 2nd step of the reaction

List of symbols

α_1	Hydrogen conversion in the 1st reaction step
α_2	Hydrogen conversion in the 2nd reaction step
α_i	Hydrogen conversion in the i reaction step
ΔH (J mol^{-1})	Enthalphy of the i step of the reaction
AB	Ammonia borane
AC	Activated carbon
B_2H_6	Diborane
$B_3N_3H_6$	Borazine
BH_2NH_2	Amminoborane
$(BHNH)_3$	Borazine
BN	Boron nitride

Entry for the Table of Contents (Please choose one layout)

Layout 1:

FULL PAPER

Ammonia borane-carbon (*AB/C*) nanocomposites can be combined with an external nickel chloride filter to release H_2 from 96 °C with no gaseous by-products detected above 100 ppb. Simulations demonstrate the suitability of *AB/C* tanks as hydrogen stores in portable power packs.

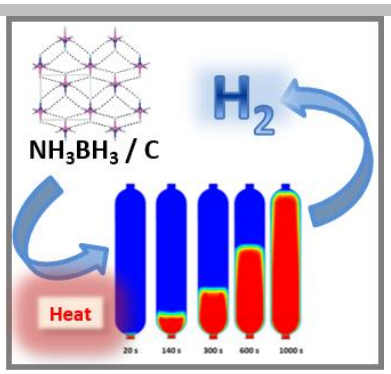

*Laura Bravo Diaz, James M. Hanlon, Marek Bielewski, Aleksandra Milewska, Duncan H. Gregory**

Layout 2:

FULL PAPER

((Insert TOC Graphic here; max. width: 11.5 cm; max. height: 2.5 cm))

*Author(s), Corresponding Author(s)**

Text for Table of Contents